*Iraqi Journal of Physics, 2026*
*https://doi.org/10.30723/ijp.v24i1.1393*

*Vol.24, No.1, PP. 31-42*
*P-ISSN: 2070-4003*
*E-ISSN: 2664-5548*

# Influence of Various CuO Nanoparticles Concentrations on Sensing Performance of ZnO Nanorods Arrays Grown Using Hydrothermal Method

**Sarah Rafid Abbas[1*] and Hind Fadhil Oleiwi[1]**
[1]*Department of Physics, College of Science for women, University of Baghdad, Baghdad, Iraq*
[*]Corresponding author: sara.rafed2304m@csw.uobaghdad.edu.iq

## Abstract
This study outlines a technique for enhancing a metal oxide semiconductor gas sensor's sensitivity to Nitrogen dioxide ($NO_2$) gas. Using a sol-gel and spin-coating process, the gas sensor was constructed from hydrothermally generated ZnO nanorods (ZNRs) and decorated with different concentrations of Copper oxide (CuO) nanoparticles (NPs). Field-emission scanning electron microscopy (FE-SEM), X-ray diffraction, and optical characteristics were used to examine the gas sensor's morphology, crystal structure, and UV-Vis absorption. The primary pattern's hexagonal structure was revealed by X-ray diffraction and FESEM images, which showed the rough surface of ZNRs/CuO NPs. $NO_2$ gas-sensing characteristics were examined at three different CuO NPs concentrations 20, 40, and 60 mg/L. The energy gap of ZNRs, ZNRs/20CuO NPs, ZNRs/40CuO NPs, and ZNRs/60CuO NPs had values of approximately 3.25, 3.25, 3.24, and 3.04, respectively. The findings showed that ZNRs decorated with CuO, compared to the non-decorated ZnO nanorods, enhanced their sensitivity to $NO_2$ gas. The highest sensitivity was at ZNRs/60CuO, reaching 140% at 150°C compared to ZNRs, ZNRs/20CuO, and ZNRs/40CuO samples.

**Article Info.**

**Keywords:**
*ZnO nanorods, drcoration, hydrothermal technique, Sensing, $NO_2$.*

**Article history:**
*Received: Oct. 30, 2024*
*Revised: Feb. 01, 2025*
*Accepted: Feb. 13, 2025*
*Published:Mar.01, 2026*

## 1. Introduction
Air pollution is a growing global concern that can harm human health and ecosystems, so identifying harmful gases is the first step in reducing air pollution. Nitrogen dioxide ($NO_2$) is the primary source of air pollution; increased $NO_2$ in the atmosphere is mostly caused by fossil fuel combustion and emissions from automobiles and factories. It is a hazardous and harmful gas, even in tiny amounts (<10 ppm). It may result in major health effects, such as coughing, eye irritation, exhaustion, and nausea [1, 2]. To protect the environment and human health; there is a great necessity to develop susceptible, selective, and responsive $NO_2$ gas-detecting devices [3]. Due to their high efficiency, metal oxide gas sensors surpass conventional devices for sensing gas concentrations in the atmosphere [4]. Metal Oxide Semiconductor (MOS) gas sensors are an appropriate choice due to their high sensitivity to target gases, small size, capability to detect many hazardous and volatile gasses under various conditions, ease of use, real-time detection, cost-effective and environmentally friendly [5, 6]. Zinc oxide (ZnO) has unique physical and chemical characteristics, making it a popular gas-sensing material for detecting toxic and harmful gases [7]. ZnO is an n-type semiconductor with high electron mobility, an exaction binding energy of 60 meV, and a direct wide bandgap (3.37 eV) at room temperature; it is non-toxic and has good chemical and thermal stability [8, 9]. One-dimensional nanomaterials, including nanorods, nanowires, nanofibers, and nanotubes, have gained major interest for their scientific value and possible applications in different devices [10, 11]. ZnO nanorods (ZNRs) are commonly employed in electronics, optoelectronics, and electronic devices, and are a good candidate for gas sensing applications [12-14].

Furthermore, it can be grown using hydrothermal techniques and can display enhanced characteristics due to its high surface area-to-volume ratios.

The hydrothermal technique is a promising method for creating unique nanomaterials due to its inexpensiveness, low temperature, excellent yield, and scalability [15, 16]. Copper oxide (CuO) is a p-type material that has a 1.2~1.8 eV band gap and outstanding physical and electrical characteristics [17] commonly used in different fields, including sensors [18], light emitting diodes [19], photocatalysts [20], and batteries [21]. CuO can form heterojunctions with n-type metal oxides, such as $CuFe_2O_4$ [22], ZnO [23], and $SnO_2$ [24]. Several studies have demonstrated the potential advantages of the p–n heterojunction created by n-type and p-type materials for the sensing process [25]. Many variables involving electrical processes have been related to the enhanced sensing ability of these composites. These include band bending as a result of Fermi level equilibration, charge carrier separation, modification of the depletion layer, and increased interfacial potential barrier energy. The improvement in sensing is also a result of the geometrical effects and chemical effects, which include greater gas accessibility, surface area enhancement, reduced activation energy, and focused catalytic activity [26].

This study used the hydrothermal method to to produce ZNRs at low cost. It investigated how different concentrations of CuO nanoparticles of the heterojunction (ZNRs/CuO) affected the properties of the heterojunction when the surface area of the heterojunction (ZNRs/CuO) increased, and how this improved the performance of the $NO_2$ gas sensor.

## 2. Materials and Methods

Sol-gel and spin-coating techniques are the first steps in fabricating a ZnO seed layer or ZNPs. To produce a sol-gel solution, equal amounts of 0.2M zinc acetate and diethanolamine (a stabilizing agent) were mixed with 8 ml ethanol. The mixture was stirred for an hour on a hot plate stirrer. The solution was kept in place for a whole day to form a stable sol. After that, the solution was applied on clean fluorine tin oxide-coated glass substrates (FTO), and the substrates were rotated at 3000 rpm for 30 seconds to form the seed layer. The thin film was heated on a hot plate for 10 min at 100 °C to eliminate any remaining ethanol; a uniform dispersion and an appropriate density of ZNPs on the substrate surface required three spin coating repetitions. After that, the samples were heated for an hour to 300 °C. Prepared seed layers were immersed in a growth solution to promote the hydrothermal growth of ZNRs. The growth solution was formed by dissolving equimolar 0.2M amounts of zinc nitrate and hexamethylenetetramine (HMT), an organic compound, in 20 ml deionized water (DI). After that, the growth solution was added to the tube, and baked for 45 min at 90 °C. Finally, the grown ZNRs were washed with DI to clear any remaining salt and organic material [27, 28]. A CuO NPs suspension was made by dissolving CuO NPs in 10 ml of ethanol. CuO NPs of different concentrations (20, 40, and 60 g/L) were deposited onto the ZNRs surface using the spin-coating method [29], and allowed to dry on a hot plate for 10 min [30]. Aluminium electrodes of about 150 nm thickness were deposited on the heterostructure using a thermal evaporation process. This resulted in a ZNRs/CuO NPs heterostructure gas sensor.

## 3. Gas Sensor Characterization

The optimal sensitivity of the ZNRs/CuONPs gas sensor was achieved by the gas sensor system configuration. This system, Fig. 1, which included many essential components, was constructed and built in the laboratory. Its first component is a stainless steel cylindrical chamber of 20 cm in diameter and 15 cm in height with three openings. Its effective capacity is 4710 $cm^3$. The opening are for the in and out signals. Conducting wires of power supply (type-DC, DAZHENG) pass thought the last final hole. The chamber is also

with gass window and a hole for loading and unloading gases. The studied samples were located inside the chamber and connected to a digital multimeter. After closing the chamber door, a 6 V alignment voltage was applied between the sample's electrodes. A rotary pump (type- EDM 12, Edwards, England) was used to evacuate the chamber to a pressure of $10^{-2}$ mbar. A thermocouple temperature controller (type-K) was used to regulate the working temperature in the range between ambient temperature and 250°C. A needle valve regulates the gas flow. A laptop PC digital multimeter (UNI-T) UT 81B completes this setup. A digital multimeter with an interface was utilized to measure gas and air flow bias resistance. Resistance was measure with no gas and as the gas flows into the system. measured. The recovery time was determined as the gas valve was switched off.

To test the samples for gas detection, the $NO_2$ gas was generated according to the reaction between $HNO_3$ acid and Cu particles, as in equation Eq. (1):

$$2HNO_3 + 2Cu \rightarrow 2NO_2 + 2CuO + H_2 \quad \textbf{(1)}$$

***Figure 1: A photograph of the gas sensor testing system.***

## 4. Results and Discussion

Field-Emission Scanning Electron Microscopy (FE-SEM) was used to examine the morphologies of both pristine ZnO NRs and ZnO NRs/CuO NPs. A smooth shape of pristine ZnO NRs was seen in the FE-SEM image of Fig. 2(a). Highly oriented and crystalline ZNR with smooth surfaces were successfully grown on FTO substrates, illustrating the successful synthesis of ZnO NRs. Additionally, images of ZnNRs decorated with CuO NPs are shown in Fig. 2 (b-d). No apparent changes in the surface morphology of hexagonally bounded nanorods under the increasing CuO concentration were noticed. The surface roughness brought on by the presence of CuO NPs was observed in the images on top of the nanorods. Agglomerated CuO NPs with irregular shapes and sizes on the surface of ZNR were perceivably found among the adjacent nanorods (as shown in the red circles in Fig. 2). These observations indirectly verify the roles of CdS in both surface modification and incorporation on the ZNRs surface. This phenomenon can be explained by a change in the density coverage of nanoparticles on the ZNR surface.

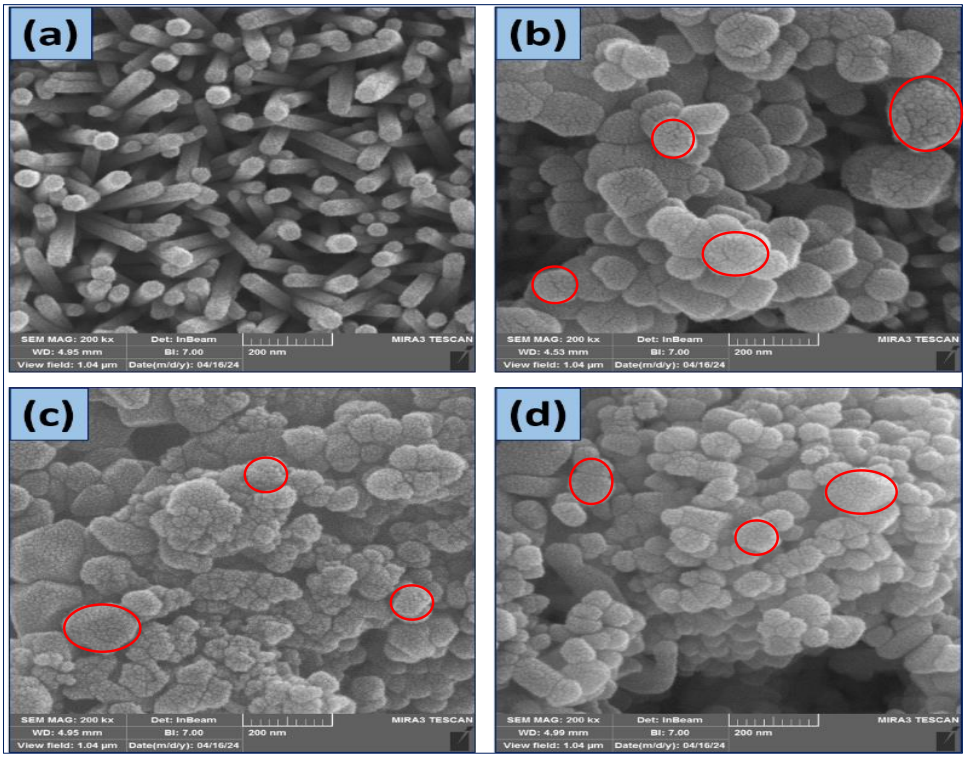


***Figure 2: FESEM images (top-view) of (a) pristine ZNRs and (b-d) ZNRs/different concentration (20, 40, and 60 g/L) of CuO NPs.***

XRD analysis determines a material's crystallinity and grain size. Fig. 3 depicts the XRD patterns of ZNRs and ZNRs/CuO NPs heterojunction at different CuO NPs concentrations. The XRD pattern of ZNRs showed peaks at 2θ of 34.27º, 47.36º, and 62.6º related to (002), (102), and (103) planes, respectively, which are consistent with (card no. 00-036-1451), and this refers to the hexagonal ZnO phase. When adding different concentrations of CuO NPs to ZNRs samples, FTO peaks disappeared whereas the primary ZnO peaks stayed unaltered; the XRD patterns showed peaks at 2θ of 35.56º, 38.68º, 48.88º, 61.48º, and 62.88º corresponding to $(11\bar{1})$, (111), $(20\bar{2})$, (11), and $(10\bar{3})$ planes, respectively, which are consistent with (card no. 00-048-1548), and this refers to the monoclinic CuO phase. This validates the deposition of CuO NPs on the ZNRs surfaces and indicates the absence of contaminants in the material, which consists only of ZnO and CuO [31, 32].

The mean crystalline size was calculated utilizing Scherer's equation [33] for ZNRs/CuO NPs, as listed in Table 1, and this demonstrates that the prepared samples include nano-sized crystals:

$$D = \frac{k\,\lambda}{\beta \cos\theta} \qquad (\mathbf{2})$$

where D represents the crystalline size (nm), k represents the Scherer constant (0.9), λ represents the wavelength of incident X-rays (0.15406 nm), θ represents the diffraction angle, and β represents the width of the peak at half the maximum height corresponding to the peak in the XRD patterns (FWHM).

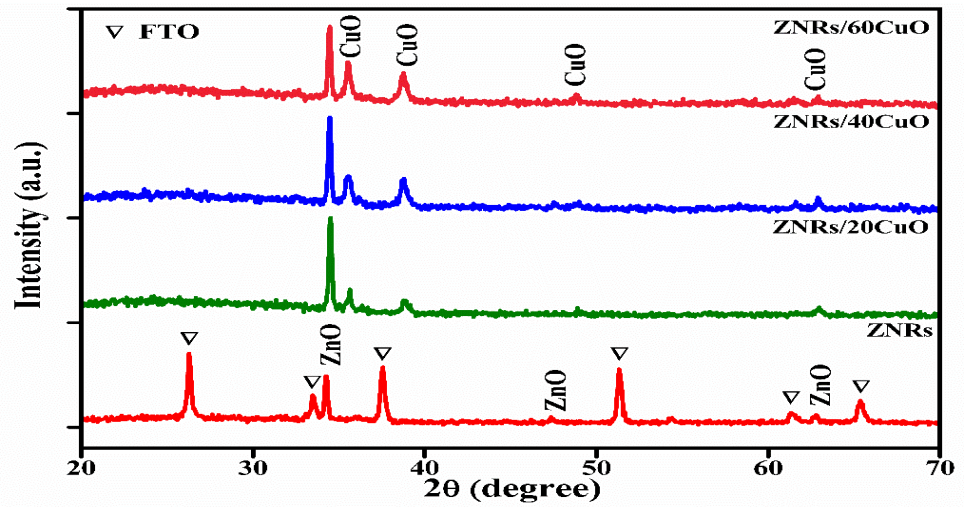


***Figure 3: XRD patterns of ZNR(bottom red line) and ZNRs with different concentrations of CuO NPs.***

***Table 1: Crystal size of ZNRs and ZNRs with different concentrations of CuO NPs.***

| Samples | 2Θ (deg) | FWHM (deg) | d ($A^0$) | D (nm) |
|---|---|---|---|---|
| **ZNRs** | 34.2756 | 0.19130 | 2.61410 | 41.5 |
| | 47.3095 | 0.17600 | 1.91987 | 45.1 |
| | 62.8634 | 0.12360 | 1.47714 | 64.2 |
| **ZNRs/20CuO** | 34.5250 | 0.19030 | 2.59579 | 41.7 |
| | 35.6491 | 0.18360 | 2.51647 | 43.2 |
| | 38.8463 | 0.31460 | 2.31640 | 25.2 |
| | 48.9367 | 0.12000 | 1.85977 | 66.2 |
| **ZNRs/40CuO** | 34.4828 | 0.19270 | 2.59887 | 41.2 |
| | 35.5668 | 0.37270 | 2.52211 | 21.3 |
| | 38.7813 | 0.37330 | 2.32013 | 21.2 |
| | 48.9162 | 0.41500 | 1.86050 | 19.3 |
| **ZNRs/60CuO** | 34.4715 | 0.19880 | 2.59969 | 39.9 |
| | 35.5593 | 0.24050 | 2.52262 | 33.0 |
| | 38.7696 | 0.38040 | 2.32080 | 20.9 |
| | 48.8291 | 0.19140 | 1.86362 | 41.5 |

The absorbance and transmittance spectra of ZnO NRs and ZnO NRs decorated with varying amounts of CuO NPs are shown in Fig. 4. A sample's absorption edge is indicated when the decreasing portion of the spectrum aligns with its baseline. From the figure, an absorption edge was noticed at wavelengths between 350 and 367 nm for all curves of ZNRs and ZNRs with different amounts of CuO NPs. This is consistent with previous research [34, 35]. The ZNRs/60CuONPs sample showed a broad absorption spectrum in the 367-450 nm region when compared to ZNRs, but the absorption spectra of the ZNRs/20CuONPs and ZNRs/40CuONPs samples did not change. As the material's surface and edge were rougher when ZnO NRs were decorated with CuO NPs, more light can be reflected and absorbed within the structure.

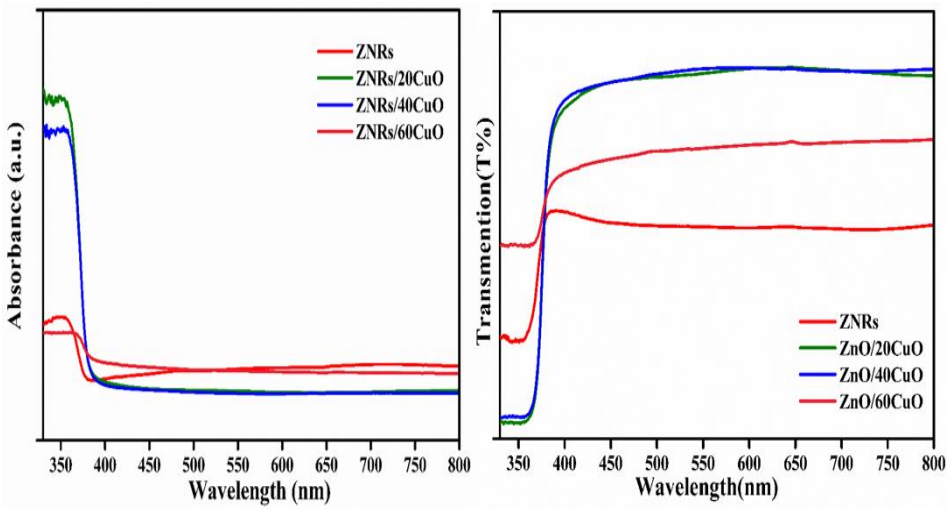


***Figure 4: Absorbance and transmittance spectra of ZNRs and ZNRs with different concentrations of CuO NPs.***

Light absorption and reflection within the structure of the decorated ZnO NRs with CuO NPs increased because the material's surface and edge were rougher than ZNRs. The presence of CuO caused an increase in absorption in the visible area. CuO redshifted light absorption so that it occurred within the visible spectrum. This redshift was attributed to a significant increase in the carrier density and the heavy doping of the samples with a superlattice structure [36]. A rise in the absorbance of ZNRs/CuO nanostructure was indicated by the increased red shift in the absorption edge that occurred as the concentration of CuO increased.

Tauc's equation was used to calculate the band gap. The ZNRs, ZNRs/20CuONPs, ZNRs/40CuONPs, and ZNRs/60CuONPs had band gap values of approximately 3.25 eV, 3.25 eV, 3.24 eV, and 3.04 eV, respectively, as shown in Fig. 5.

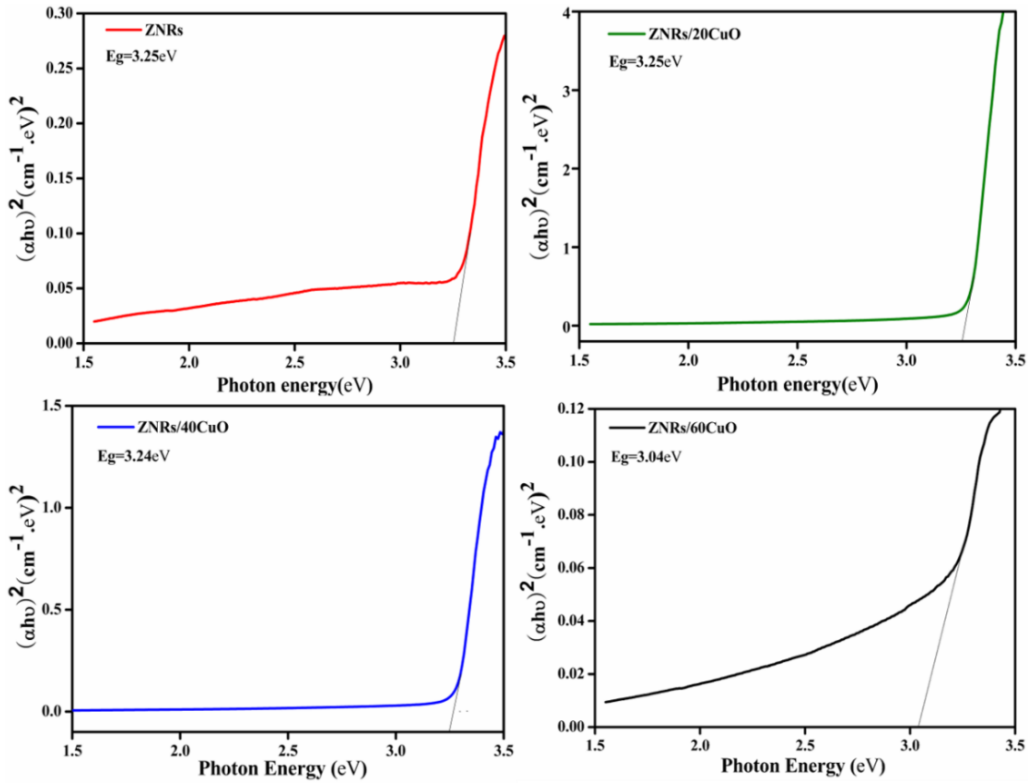


***Figure 5: Tauc plots for ZNRs and ZNRs with different concentrations of CuO NPs.***

The gas sensing characteristics were studied in a clean room with regulated temperatures of 20–25 °C and relative humidity of 40–50 %. The sensing properties of ZNRs to $NO_2$ gas were examined for different concentrations of CuO nanostructures at different temperatures to define them as gas sensors. The sensitivity, response time, and recovery time of the ZNRs and ZNRs with different concentrations of CuO gas sensors at 197 ppm $NO_2$ at different temperatures are displayed in Table 2. The sample (ZNRs/60CuONPs) started responding to $NO_2$ gas at a temperature of 70 °C with a sensing response of (96.786) as a result of its CuO NPs decoration, which caused an increase in the active sites for absorbing gas molecules. The ZNRs, ZNRs/20CuONPs, and ZNRs/40CuONPs sensors responded to $NO_2$ gas at higher temperatures and with lower sensitivity. This better sensing response of ZNRs/60CuONPs is due to the increase in the adsorption kinetics of gaseous atoms on its surface. ZNRs showed the lowest sensitivity sensitivity to $NO_2$ gas at 200°C; ZNRs/20 CuO NPs showed the highest sensitivity at 150°C; and ZNRs/60CuONPs showed the highest sensitivity at 150°C. The sensitivity of the sensor was affected because the concentration of CuO covers most of the ZNRs, leading to a reaction of competition with ZNRs.

The sensitivity % of a gas sensor is defined as the ratio of the change of the sensor resistance when exposed to $NO_2$ gas to that with no exposure, as in the following equation:

$$S\ (\%) = \frac{R_{air} - R_{gas}}{R_{air}} \times 100 \quad \textbf{(3)}$$

where $R_{air}$ represents the resistance of the sensor in air (no gas present), $R_{gas}$ represents the resistance in the presence of $NO_2$ gas.

The time needed for the sensor to react when the gas concentration fluctuates between zero and a stable value of around 90% of the final value is known as the response time. The amount of time needed for the signal from the sensor to return to its initial value after the gas flow is stopped and reaches 10% is known as the recovery time [17]. The ZNRs gas sensors' recovery and reaction time improved with the addition of CuO NPs, which also increased the gas sensor's surface area. Figs. (6-8) show the resistance change with time for ZNRs, ZNRs/20CuO, ZNRs/40CuO, and ZNRs/60CuO at different temperatures. The resistance of ZNRs increased over time, but the resistance of ZNRs decorated with different concentrations of CuO NPs decreased. ZnO NRs is an n-type material; its resistance rises as it combines with oxidizing gas ($NO_2$). In contrast, CuO NPs are a P-type substance; their resistance drops when they come into contact with $NO_2$ gas [35, 37]. For the n-type metal oxide semiconductor gas sensor, most carriers are electrons. If exposed to an oxidizing gas like $NO_2$, the sensor reacts with the oxygen ion and keeps the electrons at the surface. This decreases the electron concentration in the metal oxide and hence decrease the conductance. When the gas sensor is exposed to an ambient reducing gas, the electrons produced by the chemical reaction in the adsorbed oxygen ion formation process are returned to the conduction band [38].

The results of improving the sensitivity of the manufactured nanocomposites are displayed in Table 3, and when compared with earlier studies, this improvement in sensitivity is very noticeable.

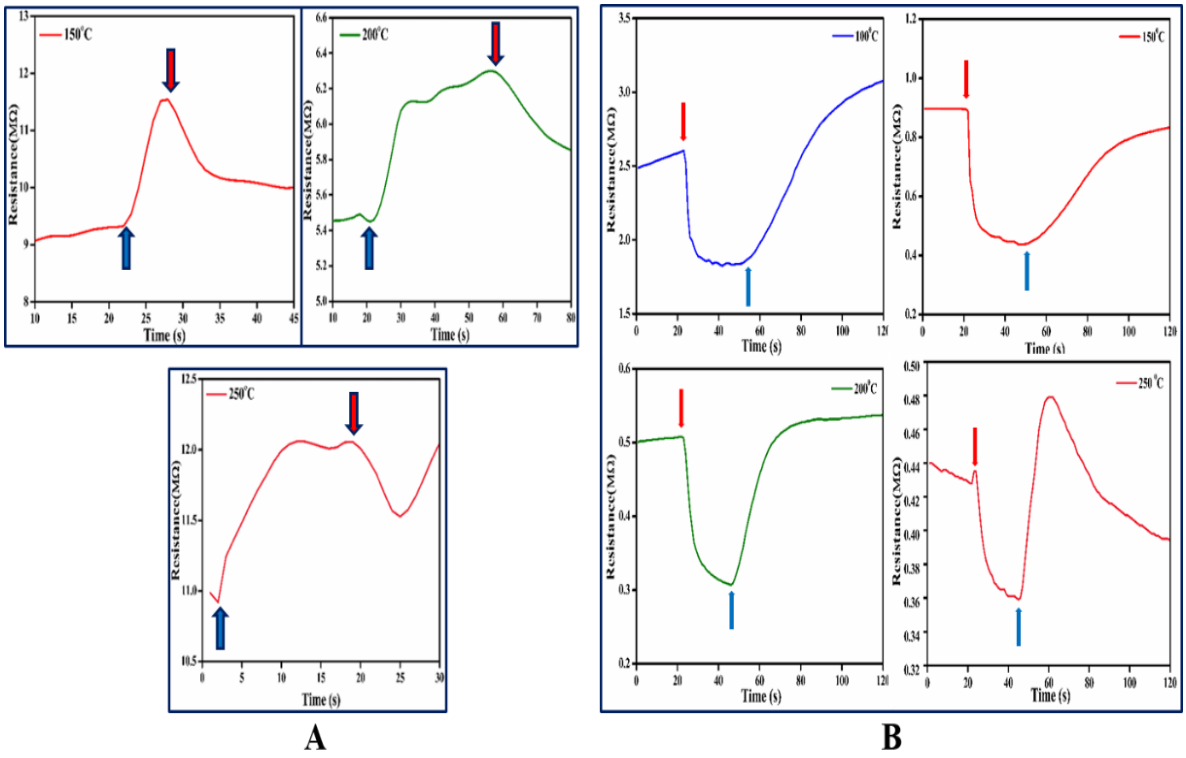


*Figure 6: Resistance with time of (A) ZNRs and (B) ZNRs/20CuONPs at different temperatures.*

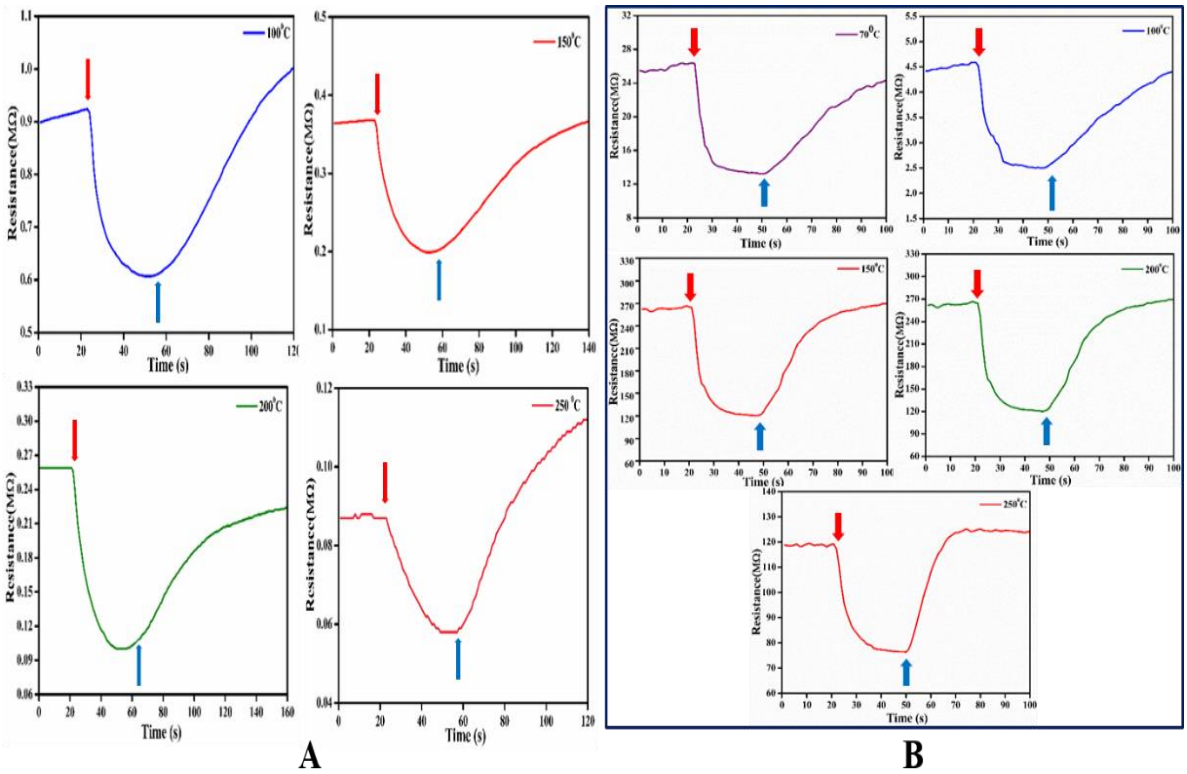


*Figure 7: Resistance with time of (A) ZNRs/40CuONPs and (B) ZNRs/60CuONPs at different temperatures.*

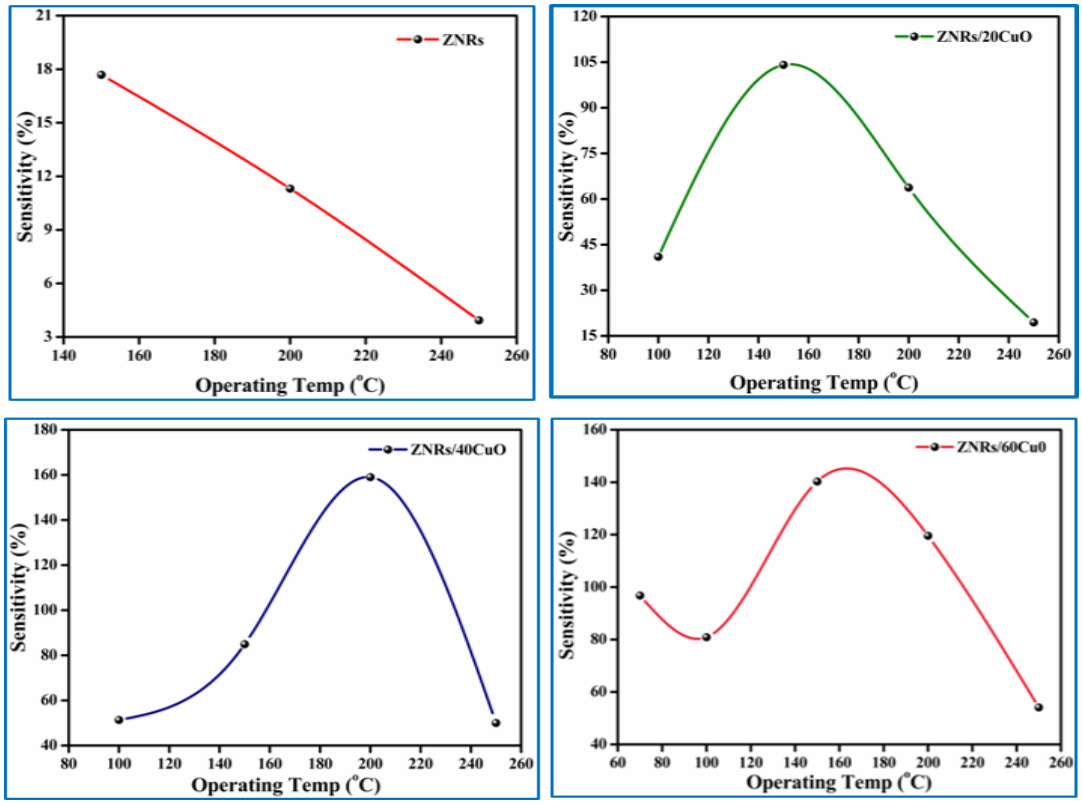


***Figure 8: Sensitivity (%) of ZNRs and ZNRs with different CuO concentrations.***

***Table 2: Sensitivity, response and recovery time of ZNRs and ZNRs with different concentration of CuO nanostructures in different temperatures.***

| Samples | Working Temperature (°C) | Sensitivity (%) | Response Time (s) | Recover Time(s) |
|---|---|---|---|---|
| **ZNRs** | 150 | 17.683 | 5.4 | 84.6 |
| | 200 | 1.309 | 19.8 | 52.2 |
| | 250 | 3.936 | 11.7 | 54.9 |
| **ZnO/20CuO** | 100 | 41.042 | 20.7 | 67.5 |
| | 150 | 104.100 | 23.4 | 66.6 |
| | 200 | 63.754 | 18.9 | 52.2 |
| | 250 | 19.444 | 21.6 | 52.2 |
| **ZnO/40CuO** | 100 | 51.311 | 22.5 | 83.7 |
| | 150 | 84.925 | 27.9 | 71.1 |
| | 200 | 159 | 27.9 | 62.1 |
| | 250 | 50 | 26.1 | 44.1 |
| **ZnO/60CuO** | 70 | 96.786 | 20.7 | 140.4 |
| | 100 | 80.876 | 23.4 | 102.6 |
| | 150 | 140.274 | 21.6 | 50.4 |
| | 200 | 119.536 | 22.5 | 40.5 |
| | 250 | 54.107 | 23.4 | 21.6 |

*Table 3: Sensing characteristics compared to earlier studies.*

| Material | Method of synthesis | Gas, conc.(ppm) | T(°C) | Response | Ref. |
|---|---|---|---|---|---|
| ZnO NRs | Hydrothermal | $NO_2$, 0.001 | 150 | 1.3 | [32] |
| ZnO NRs | Hydrothermal | $NO_2$, 100 | 150 | 113.32 | [39] |
| ZnO/CuO heterojunction | Hydrothermal | Ethanol, 100 | 300 | 98.8 | [40] |
| CuO decoration ZnO NRs | Hydrothermal | Ethanol, 100 | 350 | 68.7 | [6] |
| CuO/ZnO nanowires | Thermal oxidation | $NO_2$, 100 | 250 | 4.1 | [17] |
| CuO-ZnO nanocomposites | Chemical methods | $NO_2$, 100 | 200 | 73 | [41] |
| CuO/ZnO NRs nanocomposites | Thermal evaporation | $NO_2$, 100 | 150 | 96 | [42] |
| ZnO NRs decoration CuO NPs | Hydrothermal | $NO_2$, 197 | 200 | 159 | **This work** |

## 5. Conclusions

The ZnONRs/CuONPs heterostructure was prepared as an $NO_2$ gas sensor. Pristine ZnO NRs and ZnO NRs decorated with different CuO NP concentrations (20, 40, and 60 g/L) were successfully synthesized using hydrothermal and spin-coating techniques, respectively. When ZNRs were decorated with CuO nanoparticles, the outermost nanorods became rougher. According to XRD data, ZNRs typically have a hexagonal structure, a surface morphology, and monoclinic CuO surfaces. This investigation revealed that the sensor detected the gas at 70°C with a concentration of 60 g/L. Furthermore, all samples responded best to the gas at 200°C. The better response to the gas happens because there are more CuO NPs on the surface of ZnO NRs and because a mixed n-ZnO/p-CuO structure is formed. The relationship between nanostructure and effective gas sensor performance suggests the possibility of using it for various sorts of dangerous gas detection.

## Acknowledgements

The authors would like to thank the University of Baghdad/ College of Science for Women/ Department of Physics for their assistance in carrying out this work.

## Conflict of Interest

Authors declare that they have no conflict of interest.

## References

1. S. Tyagi, M. Chaudhary, A. K. Ambedkar, K. Sharma, Y. K. Gautam, and B. P. Singh, Sens. Diagn. **1**, 1 (2022). https://doi.org/10.1039/D1SD00034A.
2. F. Sarf, *Metal oxide gas sensors by nanostructures*, intechopen, London, UK, 2020. https://doi.org/10.5772/intechopen.88858.
3. T. Wang, J. Hao, S. Zheng, Q. Sun, D. Zhang, and Y. Wang, Nano Research, **11**,791 (2018). https://doi.org/10.1007/s12274-017-1688-y.
4. S. AbdulKareem, M. Suhail, and I. Adehmash, Iraqi J. Sci., **62**, 7 (2021). https://doi.org/10.24996/ijs.2021.62.7.7.
5. Y. Patil, R. Pedhekar, S. Patil, and F. Raghuwanshi, Materials Today: Proceedings, **28**, 1865 (2020). https://doi.org/10.1016/j.matpr.2020.05.293.
6. H. R. Madvar, Z. Kordrostami, and A. Mirzaei, Sensors, **23**, 365 (2023). https://doi.org/10.3390/s23010365.
7. S. R. Abbas and H. F. Oleiwi, J Opt, **1**, 2024. https://doi.org/10.1007/s12596-024-02341-8.

8. Y. Kang, F. Yu, L. Zhang, W. Wang, L. Chen, and Y. Li, Solid State Ionics, **360**, 115544 (2021) https://doi.org/10.1016/j.ssi.2020.115544.
9. Y.L.Chu, S.J. Young, L.W. Ji, T.T. Chu, K.T. Lam, Y.J. Hsiao, I-T. T. and T.H. Kuo, Journal of The Electrochemical Society,**167**, 117503 (2020). https://doi.org/10.1149/1945-7111/aba00d.
10. L. Wang, Y. Kang, Y. Wang, B.Zhu, S. Zhang, W. Huang, S. Wang, Materials Science and Engineering: C, **32,** 2079 (2012). https://doi.org/10.1016/j.msec.2012.05.042.
11. A. J. Rahma, H. F. Oleiwi, S. G. Khaleel and M. M. Mutter *Proceedings of the International Workshop on Nanotechnology (IWN 2020) 2020, IOP Conference Series: Materials Science and Engineering,* vol.1095, p. 012007,Al-Fallujah, Iraq. https://doi.org/10.1088/1757-899X/1095/1/012007.
12. M. R. Maurya, V. Toutam, and D. Haranath, ACS omega, **2**, 5538 (2017). https://doi.org/10.1021/acsomega.7b00914.
13. V. Kobrinsky, E. Fradkin, V. Lumelsky, A. Rothschild, Y. Komem, and Y. Lifshitz, Sensors and Actuators B: Chemical, **148**, 379 (2010). https://doi.org/10.1016/j.snb.2010.05.025.
14. D. Zhang, S. Chava, C. Berven, S. Lee, R. Devitt, and V. Katkanant, Appl. Phys. A, **100**, 145 (2010). https://doi.org/10.1007/s00339-010-5567-6.
15. L. T. Hoa, H. N. Tien, and S. H. Hur, J. Nanomater., **2014**, 710874 (2014). https://doi.org/10.1155/2014/710874.
16. H. Hu, X. Huang, C. Deng, X. Chen ,and Y. Qian, Materials Chemistry and Physics, **106**, 58 (2007). https://doi.org/10.1016/j.matchemphys.2007.05.016.
17. T.-H. Han, S.-Y. Bak, S. Kim, S. H. Lee, Y.-J. Han, and M. Yi, Sensors, **21**, 2103 (2021). https://doi.org/10.3390/s21062103.
18. A. Umar, A. Alshahrani, H. Algarni, and R. Kumar, Sens. and Actuators B: Chem., **250**, 24, (2017). https://doi.org/10.1016/j.snb.2017.04.062.
19. M. H. Barzegar, M. Ghaedi, V. M. Avargani, M. M. Sabzehmeidani, F. Sadeghfar, and R. Jannesar, Polyhedron, **158**, 506 (2019). https://doi.org/10.1016/S0022- 3093(86)80079-5.
20. H. Li, Z. Su, S. Hu, and Y. Yan, Appl. Catal. B: Environ., **207**, 134 (2017). https://doi.org/10.1016/j.apcatb.2017.02.013
21. P. S. Kumar, M. Selvakumar, S. G. Babu, S. Induja, and S. Karuthapandian, J. Alloys Compd, **701**, 562 (2017) https://doi.org/10.1016/j.jallcom.2017.01.126.
22. D. R. Miller, S. A. Akbar, and P. A. Morris, Sensors and Actuators B: Chemical, **204**, 250 (2014). https://doi.org/10.1016/j.snb.2014.07.074.
23. D. Li, L. Qin, P. Zhao, Y. Zhang, D. Liu, F. Liu, B. Kang, Y. Wang, H.Song, T. Zhang and G. Lu, Sensors and Actuators B: Chemical, **254**, 834 (2018). https://doi.org/10.1016/j.snb.2017.06.110.
24. C. Gao, Z.-D. Lin, N. Li, P. Fu, and X.-H. Wang, Acta Metallurgica Sinica (English Letters), **28**, 1190 (2015). https://doi.org/10.1007/s40195-015-0312-y.
25. Y. Xiao, Q. Yang, Z. Wang, R.Zhang, Y.Gao, P.Sun, Y. Sun and G. Lu, Sensors and Actuators B: Chemical, **227**, 419 (2016). https://doi.org/10.1016/j.snb.2015.11.051.
26. J. M. Walker, S. A. Akbar, and P. A. Morris, Sensors and Actuators B: Chemical, **286**, 624 (2019). https://doi.org/10.1016/j.snb.2019.01.049
27. Q. Li, J. Bian, J.Sun, J.Wang, Y. Luo, K. Sun and D.Yu, Appl. Surf. Sci., **256**, 1698 (2010). https://doi.org/10.1016/j.apsusc.2009.09.097.
28. N.A.M. Asib, F.S. Husairi, K.A. Eswar, A.N. Afaah, M.H. Mamat, M. Rusop and Z. Khusaimi, Sensors and Actuators A: Physical, **302**, 111827 (2020). https://doi.org/10.1016/j.sna.2019.111827.
29. H. F. Oleiwi, A. J. Rahma, S. I. Salih, and A. A. Beddai, Baghdad Sci. J., **21,** 1702 (2024). https://doi.org/10.21123/bsj.2023.8089.
30. H. F. Oleiwi and I. A. Kareem, *Ibn AL-Haitham Journal For Pure and Applied Sciences,* **36**, 137 (2023). https://doi.org/10.30526/36.4.3173.
31. M. Taufique, A. Haque, P. Karnati, and K. Ghosh, J. Electro. Mater. **47**, 6731, (2018) https://doi.org/10.1007/s11664-018-6582-1.
32. A. G. Bekru, L. T. Tufa, O. A. Zelekew, M. Goddati, J. Lee, and F. K. Sabir, ACS omega,**7**, 30908 (2022). https://doi.org/10.1021/acsomega.2c02687.
33. G. W. Scherer, J. Non-Cryst. Solids, **87,** 99 (1986). https://doi.org/10.1016/S0022- 3093(86)80079-5.
34. N. M. Vuong, N. D. Chinh, B. T. Huy, and Y.-I. Lee, Sci. rep., **6,** 26736 (2016). https://doi.org/10.1038/srep26736.
35. D.N. Giang, N. M. Nguyen, D. A. Ngo, T. T. Tran, L. T. Duy, C. K.Tran, T. T. V. Tran, P. P. H. La and V. Q. Dang, Beilstein Journal of Nanotechnology, **14**,1018 (2023). https://doi.org/10.3762/bjnano.14.84.
36. A. B. Djurišić and Y. H. Leung, Small, **2,** 944 (2006). https://doi.org/10.1002/smll.200600134.
37. N. Vuong, N. Chinh, B. Huy, and Y. Lee, Sci. Rep. **6**, 26736 (2016), https://doi.org/10.1038/srep26736.
38. A. Dey, Materials science and Engineering: B, **229**, 206 (2018). https://doi.org/10.1016/j.mseb.2017.12.036
39. S. B. Jagadale, V. L. Patil, S. A. Vanalakar, P. S. Patil, and H. P. Deshmukh, Ceramics International,**44**, 3333 (2018). https://doi.org/10.1016/j.ceramint.2017.11.116.

40. Y.-B. Zhang, J. Yin, L. Li, L.-X. Zhang, and L.-J. Bie, Sensors and Actuators B: Chemical, **202**, 500 (2014). https://doi.org/10.1016/j.snb.2014.05.111.
41. S.M. Mali, S. S. Narwade, Y. H. Navale, S. B. Tayade, R. V. Digraskar, V. B. Patil, A. S. Kumbhar and B. R. Sathe, ACS omega, **4**, 20129 (2019). https://doi.org/10.1021/acsomega.9b01382.
42. Y. Navale, S. Navale, M. Chougule, N. Ramgir, and V. Patil, J Mater Sci: Mater Electron, **32**, 18178 (2021). https://doi.org/10.1007/s10854-021-06360-0.

# تأثير تراكيز مختلفة من جسيمات أوكسيد النحاس النانوية على أداء الاستشعار لقضبان أوكسيد الزنك النانوية النامية باستخدام الطريقة الحرارية المائية

**سارة رافد عباس[1] وهند فاضل عليوي[1]**
*[1]قسم الفيزياء، كلية العلوم للبنات، جامعة بغداد، بغداد، العراق*

## الخلاصة
تتناول هذه الدراسة تقنية لتعزيز حساسية مستشعر غاز أشباه الموصلات من أوكسيد المعدن لغاز $NO_2$. باستخدام طريقة السول-جل والطلاء الدوراني، تم إنشاء مستشعر الغاز من قضبان نانوية من أوكسيد الزنك (ZNRs) المولدة حرارياً ومغطاة بتراكيز مختلفة من جسيمات أوكسيد النحاس (CuO NPs) النانوية. تم استخدام المجهر الإلكتروني الماسح للانبعاث الميداني (FE-SEM) والحيود بالأشعة السينية والخصائص البصرية لفحص مورفولوجيا مستشعر الغاز والبنية البلورية وامتصاص الأشعة فوق البنفسجية المرئية. تم الكشف عن البنية السداسية للنمط الأساسي من خلال حيود الأشعة السينية وصور FESEM التي تُظهر السطح الخشن لجسيمات أكسيد الزنك النانوية. تم فحص خصائص استشعار غاز ثاني أكسيد النيتروجين لجسيمات أكسيد النحاس النانوية عند ثلاثة تركيزات مختلفة 20 و40 و60 مجم / لتر. كانت قيمة فجوة الطاقة لجسيمات ZNRs وZNRs/20CuO NPs وZNRs/40CuO NPs وZNRs/60CuO NPs على التوالي 3.25 و3.25 و3.24 و3.04 تقريبًا. وأظهرت النتائج أنه بالمقارنة مع قضبان ZnO النانوية غير المزخرفة، فإن تزيينها بأكسيد النحاس عزز حساسيتها لغاز ثاني أكسيد النيتروجين. وكانت أعلى حساسية عند ZNRs/60CuO، حيث وصلت إلى 140% عند 150 درجة مئوية مقارنة بعينات ZNRs وZNRs/20CuO وZNRs/40CuO.

**الكلمات المفتاحيه:** قضبان نانوية من أكسيد الزنك، التزيين، تقنية الحرارة المائية، الاستشعار، ثاني أكسيد النيتروجين.